3D Chemical Shift-Encoded MRI for Volume and Composition Quantification of Abdominal Adipose Tissue During an Overfeeding Protocol in Healthy Volunteers

Angeline Nemeth, Berenice Segrestin, Benjamin Leporq, Kévin Seyssel, Khuram Faraz, Valerie Sauvinet, Emmanuel Disse, Pierre-Jean Valette, Martine Laville, Hélène Ratiney, et al.

Title: 3D chemical shift-encoded MRI for volume and composition quantification of abdominal adipose tissue during an overfeeding protocol in healthy volunteers

Author Names and Degrees:

Angeline Nemeth[1], MS, Bérénice Segrestin[2,3], MD, Benjamin Leporq[1], PhD, Kevin Seyssel[4], PhD, Khuram Faraz[1], PhD, Valérie Sauvinet[2], MS, Emmanuel Disse[2,3], MD-PhD, Pierre-Jean Valette[5], MD-PhD, Martine Laville[2,3], MD-PhD, Hélène Ratiney[1], PhD, and Olivier Beuf[1], PhD

Author Affiliations:

[1]Univ Lyon, INSA-Lyon, Université Claude Bernard Lyon 1, UJM-Saint Etienne, CNRS, Inserm, CREATIS UMR 5220, U1206, F69621, Lyon, France, [2]Centre de Recherche en Nutrition Humaine Rhône-Alpes (CRNH-RA), Centre Hospitalier Lyon Sud, Pierre-Bénite, Lyon, France, [3]Institut National de la Santé et de la Recherche Médicale Unit 1060, CarMeN Laboratory , Lyon 1 University, Oullins, France, [4]Department of Physiology, Faculty of Biology and Medicine, University of Lausanne, Lausanne, Switzerland, [5]Hospices Civils de Lyon, Département d'imagerie digestive, CHU Edouard Herriot, Lyon, France

Correspondence to:

Olivier Beuf, Univ Lyon, INSA-Lyon, Université Claude Bernard Lyon 1, UJM-Saint Etienne, CNRS, Inserm, CREATIS UMR 5220, U1206, F69621, Lyon, France

Email: Olivier.beuf@creatis.insa-lyon.fr

Grant Support:

LABEX PRIMES (ANR-11-LABX-0063), the "Investissements d'Avenir" program ANR-11-IDEX-0007, IHU OpéRa (ANR-10-IBHU-0004).

Running Title: Quantification of adipose tissue by CSE-MRI

Abstract

BACKGROUND

Overweight and obesity are a major worldwide health concern characterized by an abnormal accumulation of fat in adipose tissue (AT) and liver.

PURPOSE

To evaluate the volume and the fatty acid (FA) composition of the subcutaneous adipose tissue (SAT) and the visceral adipose tissue (VAT) and the fat content in the liver from 3D CSE-MRI acquisition, before and after a 31 days overfeeding protocol.

STUDY TYPE

Prospective and longitudinal study.

SUBJECTS

21 non-obese healthy male volunteers

FIELD STRENGTH/SEQUENCE

A 3D spoiled-gradient multiple echo sequence and STEAM sequence were performed at 3T.

ASSESSMENT

AT volume was automatically segmented on CSE-MRI between L2 to L4 lumbar vertebrae and compared to the DEXA measurement. CSE-MRI and MRS data were analyzed to assess the proton density fat fraction (PDFF) in the liver and the FA composition in SAT and VAT. Gas chromatography-mass spectrometry (GC-MS) analyses were performed on 13 SAT samples as a FA composition countermeasure.

STATISTICAL TESTS

Paired t-test, Pearson's correlation coefficient and Bland Altman plot were used to compare measurements.

RESULTS

SAT and VAT volumes significantly increased ($p<0.001$). CSE-MRI and DEXA measurements were strongly correlated ($r=0.98$, $p<0.001$). PDFF significantly increased in the liver (+1.35, $p=0.002$ for CSE-MRI, +1.74, $p=0.002$ for MRS). FA composition of SAT and VAT appeared to be consistent between localized-MRS and CSE-MRI (on whole segmented volume) measurements. Significant difference between SAT and VAT FA composition was found ($p<0.001$ for CSE-MRI, $p=0.001$ for MRS). MRS and CSE-MRI measurements of the FA composition were correlated with the GC-MS results (for ndb: $r_{MRS/GC-MS}=0.83$ $p<0.001$, $r_{CSE-MRI/GC-MS}=0.84$, $p=0.001$; for nmidb: $r_{MRS/GC-MS}=0.74$, $p=0.006$, $r_{CSE-MRI/GC-MS}=0.66$, $p=0.020$)

DATA CONCLUSION

The follow-up of liver PDFF, volume and FA composition of AT during an overfeeding diet was demonstrated through different methods. The CSE-MRI sequence associated with a dedicated post-processing was found reliable for such quantification.

Key words (3 to 6): Fatty acid composition, in vivo, MR spectroscopy, chemical shift-encoded imaging, overfeeding, gas chromatography-mass spectrometry

Terminology

- AT, adipose tissue
- FA, fatty acid;
- SFA, saturated fatty acid;
- MUFA, monounsaturated fatty acid;
- PUFA, polyunsaturated fatty acid;
- *ndb*, number of double bonds;
- *nmidb*, number of methylene-interrupted double bonds;
- SFA_{indx}, proportion of saturated fatty acid estimated by *ndb* and *nmidb*;
- $MUFA_{indx}$, proportion of monounsaturated fatty acid estimated by *ndb* and *nmidb*;
- $PUFA_{indx}$, proportion of polyunsaturated fatty acid estimated by *ndb* and *nmidb*;
- CL, chain length;
- SAT, subcutaneous abdominal adipose tissue;
- VAT, visceral adipose tissue;
- PDFF, proton density fat fraction
- CSE-MRI, chemical shift-encoded magnetic resonance imaging
- CV, coefficient of variation
- GC-MS, gas chromatography-mass spectrometry
- IFCC, International Federation of Clinical Chemistry
- TAG, triacylglycerol
- SNR, signal to noise ratio

Text (5199words):

INTRODUCTION

Obesity is a complex disease combining genetic factors still poorly identified and environmental factors mainly related to diet and physical inactivity(1). Overweight and obesity are major worldwide health issues increasing the risk to develop pathologies such as diabetes, cardiovascular disease and Non Alcoholic Fatty Liver Diseases (NAFLD). Although obesity is defined by a body mass index (BMI) greater than or equal to 30 kg/m^2 for humans, distribution of adipose tissue is decisive in the assessment of cardio-metabolic risk factors(2). People with abdominal fat accumulation have commonly an altered metabolic profile (also called metabolic syndrome). The expansion of visceral adipose tissue (VAT), leading to an increase in waist circumference, is associated with a higher risk to develop insulin resistance and type 2 diabetes unlike the expansion of subcutaneous adipose tissue (SAT) (3). BMI is not relevant to predict these risks because no distinction is made between fat mass and lean mass. Dual-energy X-ray absorptiometry (DEXA) allows measurement and distribution of body fat. To be more accurate, some imaging modalities like Magnetic Resonance Imaging (MRI) and computed tomography (CT) (4) can assess independently the distribution of SAT and VAT unlike DEXA. The major drawback of CT is the ionizing radiation exposure of patients whereas MRI allows the measurement of fat volumes without any known short- or long-term side effects. Over the last decades, various segmentation methods of SAT and VAT volume have emerged based on various MRI acquisition such as T1-weighted, T2-weighted or chemical-shift encoded imaging (CSE-MRI), each one with advantages and disadvantages (5). T1-weighted and T2-weighted image contrast varies with B0 field strength which can be a problem in the reproducibility of the results in multi-center studies. CSE-MRI can give an accurate estimate of proton density fat fraction (PDFF) which is a biomarker (6). Beyond volume quantification, the lipid composition of these tissues could be a relevant biomarker

(7).When analyzed by mass spectrometry (8), fatty acid composition (FA) of AT has been associated with AT function (adipogenesis, differentiation, lipid metabolism) with large differences between SAT and VAT, shedding light on the pathophysiology of metabolic diseases(8, 9).This analysis requires access to human tissue, and cannot be widely proposed. Surrogate markers of lipid composition of AT are needed. Magnetic Resonance Spectroscopy (MRS) is able to provide non-invasively the proportions of saturated (SFA), monounsaturated (MUFA) or polyunsaturated (PUFA) fatty acids. Recent studies (10–12) demonstrated the feasibility of assessing the composition of fat based on multiple gradient echo imaging also named chemical shift-encoded MRI (CSE-MRI). Studies focusing on liver diseases have extensively compared the MRS and MRI methods for the quantification of the PDFF (13–15).

The aim of this work was to assess CSE-MRI method to detect content and composition changes of fat storage in healthy volunteers during a 31 days overfeeding protocol while comparing CSE-MRI results with DEXA, MRS and GC-MS measurements.

MATERIALS AND METHODS

Overfeeding Protocol

From February 2014 to December 2016, volunteers were recruited via notice boards and electronic bulletins. To be eligible, participants had to be a man aged between 18 and 55 years with a BMI between 23.0 kg/m^2 and 27.0 kg/m^2 and low physical activity. Volunteers were excluded if they had personal medical history of type 1 or 2 diabetes. Written informed consent was obtained from all the subjects. All men underwent 31 days of high-sucrose and high-fat overfeeding by eating the equivalent of +50% of their daily energy requirements while maintaining their eating and sport activity habits. This protocol was validated by an ethics committee and was registered on the clinicaltrials.gov site (NCTXXXXXXXX). Only results from subjects with a placebo complement to their eating are reported in this paper.

Imaging And Spectroscopy Protocol

MRI

Subjects underwent two 3D spoiled-gradient multiple echo sequence on a 3T Ingenia Philips system (Philips Healthcare, Best, the Netherlands): one before the overfeeding at day 0 (MRI1) and the second at day 31 (MRI2). 3D MRI acquisitions parameters were the following : 8 echoes (n x 1.15 ms TE with n=1, …,8), 5° flip angle, 10.3 ms TR, 384 x 420 x 320 mm^3 FOV, 256 x 256 x 80 matrix size, 20.8 s scan time. This acquisition was made in breath-holding. The subjects were in supine position with both arms aligned along the body. For signal reception, a 32-channel abdominal body-array coil was used. The acquisition was performed on the abdominal region, encompassing L1 to L5 lumbar vertebrae and the liver.

DEXA

Fat weight and lean weight were determined by dual-energy X-ray absorptiometry (DEXA, Lunar Prodigy GE Medical Systems). Subjects underwent two whole-body DEXA scanning: one before the overfeeding (day-7 or day 0) and the other after the overfeeding (day 28 or day 31). Fat weight of android region from DEXA was compared to CSE-MRI measurement. The android region was the area between the ribs and the pelvis (top of the iliac crest)(16) and was close to the defined region in MRI method.

Spectroscopy

Subjects underwent two STEAM sequences in a row for test-retest using respiratory triggering with voxel placed in liver, VAT and SAT tissues (parameters in the caption of Figure 1). This protocol was performed at the baseline examination (MRS1) and repeated after the overfeeding (MRS2).

FA Analysis By Gas Chromatography-Mass Spectrometry (GC-MS)

The total FA compositions of the SAT samples were determined independently by GC-MS. FAs profiles were obtained from the triacylglycerol (TAG) fraction which is representative of the intracellular content of the SAT.

Sample Collect

A needle biopsy of abdominal SAT was performed 10cm from the umbilicus, under local anesthesia (1% lidocaine, BD microlance 21G $1^{1/2}$ inch,0.8*40mm needles), for 300mg to 1g adipose tissue samples. Subsequent biopsy was taken contralaterally. Fat samples were immediately frozen in liquid nitrogen and stored at -70 °C.

Sample Preparation

Approx. 50 mg cryogenically crushed sample were weighed exactly before proceeding to the total lipid extraction using 6 mL of a mixture of chloroform/methanol (2:1, vol:vol) according to the Folch method (17). An internal standard (TAG C17:0, glycerol triheptadecanoate), corresponding to 60µg of C17:0 /mg of tissue, was added in order to quantify the FAs occurring from the TAG fraction. The TAG fraction was then obtained from 1/40e of the total lipid extract by thin-layer chromatography on silica-gel plates with a mobile phase of hexane: diethyl ether:acetic acid (80:20:1, vol:vol:vol) and was submitted to direct methylation according to a modification of the technique described elsewhere (18).

GC-MS Analysis

The amounts of FAs were measured by GC/EI-MS (EI: electron ionization) using a quadrupole mass spectrometer (model MS 5975, Agilent Technologies, Massy, France) connected to a gas chromatograph (model GC6890, Agilent Technologies) equipped with a fused-silica column (SP2380, 60 m x 0.20 mm x 0.25 µm film thickness; Supelco). Injection (1 µL) was performed in splitless mode at 240 °C. FAs were separated with the following

oven program: (a) 50 °C for 1 min; (b) increase at a rate of 20 °C.min^{-1} to 175 °C and hold for 9.75 min; (c) increase at a rate of 2 °C.min–1 to 217 °C and hold at 217 °C for 1 min. Mass spectra were obtained from the Total Ion Chromatogram (TIC) over a mass range of m/z 35–450.

Comparison With NMR Methods

In order to obtain comparable results between the GC-MS and NMR methodologies, the mean number of double bound (ndb_{GC}) and the mean of methylene-interrupted double bound ($nmidb_{GC}$) by triglyceride chain were computed as:

$$ndb_{GC} = \left(\sum_{i}^{N} ndb_i * p_i\right) * 3$$

$$nmidb_{GC} = \left(\sum_{i}^{N} nmidb_i * p_i\right) * 3$$

$$CL_{GC} = \left(\sum_{i}^{N} CL_i * p_i\right)$$

Where N was the number of the different type of FAs analyzed, ndb_i number of double bound of the ith FA, $nmidb_i$ number of methylene-interrupted double bound of the ith FA, CL_i the number of carbon in FA chain and p_i the relative proportion of the ith FA.

MRS Signal Processing And Analysis

For spectrum acquired in SAT, similarly to the eddy current correction performed usually using the water phase signal, the time dependent phase variation of the signal of the first echo (TE=14ms) was corrected with the time dependent phase of the second echo (TE=24ms) which was less impacted by eddy current effects. This correction was possible because 1) the methylene -CH_{2n}- amplitude peak was the unique preponderant component, and 2) $\Delta TE=TE_2$-

TE_1 was small compared to the lipid T2 and 1/J ($4 < J < 8$Hz, for in vivo FA spectral). This correction needs exactly the same frequency content in the two spectra. So it was not applied to the spectra from the VAT tissue because of the presence of a low water peak in some case. In this latter case, the signal is probably altered due to peristalsis of the digestive tract from one echo to the other which could explain why the water peak contribution varies from one echo to the other. The quantification method, described shortly below and in (19), was applied only on the spectrum of the first echo; the other echoes were acquired to estimate the $T2_k$s, i.e the apparent T2 of each resonating lipid component ($k \in [1,\ldots,10]$). $T2_k$ estimations were made in the frequency domain, for each resonance, with a nonlinear least-square estimation of the mono-exponential $S_k(TE) = S0_k * \exp(-TE/T2_k)$, where $S_k(TE)$ was the measured integral of the k^{th} peak at TE (6 echoes varying regularly from 14ms to 64ms by step of 10ms), $S0_k$ the amplitude at TE=0 and $T2_k$ the T2 of the k^{th} peak.

To quantify the PDFF in the liver, a Voigt (20) model with 2 peaks was applied on the spectrum to estimate the amplitude of the water peak at 4.7ppm and the main peak of fat at 1.3 ppm. The PDFF was then computed by $PDFF = A_f/(A_w + A_f)$. The non-linear least square optimization of the Voigt model was applied on the 200 first points of the FID (~100ms and omitting the first point).

The MRS results reported in the rest of the paper are the mean quantification values of the two consecutive acquisitions.

CSE-MRI Processing And Analysis

Automated Segmentation Method Of SAT And VAT

Automatic segmentation was simultaneously performed exploiting the PDFF mapping described in (21) as well as the first and second echo images (out of phase and in phase respectively) to separate SAT from VAT. An operator determined the slices corresponding to

the upper of L2 and the lower of L4. A first reference slice chosen by the user in the stack of images was segmented automatically. Manual correction can be done if necessary. Thanks to 3D acquisition and low partial volume effect, the mask of a slice (reference slice for the beginning) was used as *a priori* knowledge for the determination of the next slice mask using the *Lankton* level set algorithm (22). After segmentation, two binary masks were created one for SAT and the other for VAT and multiplied to the PDFF map ($PDFF_{SAT}$ and $PDFF_{VAT}$ map). Only pixels with a PDFF higher than 55% were kept in order to remove vertebrae and intramuscular adipose tissue contributions to VAT volume. In some regions of large static field inhomogeneity, at the level of iliac crests, fat/water swaps led to erroneous PDFF contribution in particular in SAT. In this case, a manual correction was made.

SAT, VAT And TAT Volumes

The SAT and VAT masks were binary images. The total abdominal adipose tissue (TAT) was calculated by adding the SAT and VAT masks. Adipose tissue volumes were calculated by counting all pixels in the mask of SAT (or VAT or TAT) considering that each pixel represented 100% of fat and multiplying by the elementary volume (voxel of $9.84\ 10^{-3}\ cm^3$). The total abdominal adipose tissue (TAT) volume delimited by the L2 and L4 vertebrae was converted into mass using the assumed an average density of $0.92\ g/cm^3$ (23) and compared to the DEXA measurement on android region. The total fat content in android region considering the PDFF of the tissues (adipose tissues, muscles and vertebrae) was also analyzed and computed as the sum of each element of the matrix defined by $(PDFF_{SAT}+PDFF_{VAT}) * 9.84\ 10^{-3}\ cm^3 * 0.92 g/cm^3$.

Fat Content In The Liver

The region of interest (ROI) in the liver was manually defined on a unique slice on which the right hepatic portal vein appeared the largest in axial plane. The mean value of PDFF in this ROI was computed. To compare CSE-MRI and MRS measurements, the mean PDFF value

was computed in an ROI corresponding to the MRS voxel size and labeled "localized CSE-MRI measurement". This ROI was located automatically on the CSE-MRI data using MRS voxel coordinates. MRI was acquired in breath-holding whereas MRS was in free breathing. This difference led to localization errors of ROI on CSE-MRI. Thus, a manual ROI repositioning was visually performed in the liver.

Calculation Of FA Composition (CSE-MRI And MRS)

To avoid any difference linked to data processing, the FA quantification method used the same model function and implementation for CSE-MRI (10) and MRS (19). Indeed, in this previous publication (19), it has been shown that, despite different J-evolutions between STEAM sequence and 3D CSE-MRI, the model used in CSE-MRI can be used for MRS data analysis and lead to consistent results. FA composition was determined by a fitting procedure applied in the time domain on specific points defined by the methylene chemical shift: t = t=n*t_e with $t_e = \pi/((4.7\text{-}1.3)*B_0*\gamma)$ = 1.15 ms and n=1,...,32 for MRS processing and n=1, …,8 for CSE-MRI. The model function used was defined as:

$$f(t) = \text{real}\left((\text{Aw} * n_{water} * e^{-\frac{(TE+t)}{T2w}} + Af * \sum_{k=1}^{8} \left(n_k(ndb, nmidb, CL) * e^{2\pi i \Delta f_k t} * e^{-\frac{(TE+t)}{T2_k}} \right)) * e^{-\frac{t}{T2'}} \right)$$

where Aw and Af represent the numbers of water and triglycerides molecules respectively, n_k(ndb, CL, nmidb) the number of protons in the fat spectrum component k in terms of ndb, CL and nmidb (Table 1), f_k the frequency shift between water and each fat spectrum component k, n_{water} the number of protons in a water molecule, $T2_k$ the transverse relaxation of the k^{th} peak, $T2_w$ the transverse relaxation of the water peak, and the T2' the global

relaxation time decay induced by B0 dispersion. For MRS processing, the $T2_k$-values were estimated before the fitting and T2' was estimated during the processing (TE = 14 ms). For CSE-MRI processing, the global apparent T2* (1/T2*=1/T2+1/T2') value was computed (TE = 0 ms). FA composition was derived from ndb and nmidb with the following relations (11):

$$PUFA_{indx} = \frac{nmidb}{3} * 100$$

$$MUFA_{indx} = \frac{(ndb - 2 * nmidb)}{3} * 100$$

$$SFA_{indx} = 100 - PUFA_{indx} - MUFA_{indx}$$

$PUFA_{indx}$ is the relative proportion of polyunsaturated FA, $MUFA_{indx}$ the relative proportion of mono-unsaturated FA and SFA_{indx} the relative proportion of saturated FA.

The CSE-MRI measurement of $PUFA_{indx}$ (respectively $MUFA_{indx}$ and SFA_{indx}) was calculated on whole-segmented volume of SAT (respectively VAT). To see the influence of the inhomogeneity of the B0 field, another calculation was also computed excluding pixels at the boundary between air/water or fat interface and pixels with an estimation of T2* under 10 ms (figure 1 in supplementary material).

Statistical Analysis

Anthropometric measurements are expressed as mean ± SEM. Pearson's correlation coefficient and Bland Altman plot were used to compare reference measurements (DEXA or MRS) and CSE-MRI measurements. Coefficient of variation (CV) was computed to analyze the variability of the measurements. Paired t-tests were performed to compare data from MRI1 (or MRS1) and MRI2 (or MRS2) for each quantified parameters (PDFF in the liver, volume and FA composition of AT). The normality of each data distribution was tested using the Shapiro-Wilk test. In the case of non-normal distribution, a paired sample Wilcoxon rank

test (non-parametric test) was performed in addition to the t-test. P-value <0.05 was considered as significant. Statistical analyses were made with the software OriginPro 8.5.1 SR2 (OriginLab Corporation, Northampton, England).

RESULTS

Subjects

Baseline characteristics of 21 non-obese healthy male volunteers are summarized on Table 2. An MRI examination after overfeeding could not be performed for one subject and the MRS acquisitions from another subject before overfeeding were missing.

Volumes

MRI vs DEXA Before Intervention

On a total of 21 subjects, 18 underwent DEXA scanning on the same device (DEXA, Lunar Prodigy GE Medical Systems) and three on a different one (Discovery A, Hologic, Bedford, MA, USA). Only data from the first 18 subjects were used for the comparison. An excellent correlation between CSE-MRI measurement of TAT and DEXA measurement of android region ($r = 0.98$, $p < 0.001$) was found with a constant lower value of MRI-based estimate (bias of -120g, Bland-Altman plot Figure 2). This bias represented 6% in average of the android region mass. The total fat content measured by CSE-MRI considering PDFF of tissues was also highly correlated to DEXA measurement of android region ($r=0.94$, $p<0.001$, bias of +96g).

After The Overfeeding Intervention

The subjects gained 2.5 ± 0.3kg, with a 1.6 ± 1.1kg total fat mass gain measured by DEXA (Table 2). SAT, VAT and TAT volumes quantified using CSE-MRI sequence significantly increased between the two examinations (+91 cm^3, $p<0.001$; +129 cm^3, $p<0.001$; +219 cm^3, $p<0.001$ respectively). A significant increase in fat mass measured by DEXA in android

region was also observed (+191 g, p=0.001) and was correlated to the CSE-MRI measurements of TAT (r=0.80, p<0.001, n=16). The ratio VAT/SAT also significantly increased after overfeeding (+0.06, p=0.020).

Fat Content In Ihe Liver

Hepatic fat content is low in healthy subjects and difficult to detect. In some MRS measurements, fat content could not be detected: 2/20 at the baseline (MRS1). Over the total of 21 subjects at baseline, one subject presented an abnormal level of PDFF in the liver (PDFF>10%) based on CSE-MRI measurements (Figure 3a). Surprisingly, its corresponding MRS measurement indicated a normal level of PDFF (PDFF=3.33%). This subject had a non-homogeneous (figure 2 in supplementary material) fat content in the liver and the MRS measurement was made in a low-fat region of the liver.

Liver PDFF: MRI vs MRS

At baseline, the correlation between localized CSE-MRI and MRS measurements was poor (r^2 = 0.50, y=1.02x+0.57). In Addition, the localized CSE-MRI gave larger PDFF-values (+0.60 percentage points). After the overfeeding, the correlation was improved (r^2 = 0.80, y=1.04x+0.42) with still a lager value of CSE-MRI PDFF measurements (+0.55 percentage points). Interestingly, even if the CSE-MRI seemed to give larger PDFF-values in the case of low-fat content, variations of PDFF between the two examinations measured by MRS or CSE-MRI were found to be very close (r^2 = 0.77, y=0.92x+0.09). Moreover, the bias between these two measurements was small (larger value of localized CSE-MRI +0.05 percentage points, Bland-Altman Figure 4). The Figure 4 shows an outlier point with a ΔMRS (MRS2-MRS1) PDFF value at 3.37 and a ΔMRI (MRI2-MRI1) PDFF value at 0.39. We must notify that the two subsequent MRS2 acquisitions of the subject gave significantly (p<0.001) different results: 6.32% at the first acquisition and 2.46% at the second acquisition. If we

excluded this first acquisition and kept only the second, the MRS2-MRS1 value would be consistent with other points ($r^2 = 0.85$, $y=0.98x+0.08$, bias of 0.05).

Liver PDFF: After The Overfeeding Intervention

MRS measurements indicated that the PDFF in liver increased significantly (+1.74, paired t-test p=0.002) between the two examinations. Similarly, for CSE-MRI measurements, the PDFF in liver increased significantly (+1.35, paired t-test p=0.002). As shown in the Figure 3a and 3c, data had a non-normal distribution (Shapiro-Wilk test $p<0.001$ for MRS1; $p<0.001$ for MRS2; $p<0.001$ for MRI1; $p<0.001$ for MRI2) and a non-parametric test (paired sample Wilcoxon rank test) was performed (same observation: positive difference for MRS2-MRS1 $p<0.001$ and positive difference for MRI2-MRI1 $p<0.001$).

FA Composition Of VAT And SAT

Some VAT spectra were not analyzed due to poor quality of spectra (low SNR or high inhomogeneity of B0 field) and were removed from the analyses: 4/20 at baseline and 3/21 after overfeeding. The CSE-MRI data of one subject could not be processed to estimate the FA composition.

FA Composition: Variabilities

For CSE-MRI measurement at the first examination, the intra-subject variability was high with a larger heterogeneity of nmidb values in VAT (mean CV of: ndb 28%, nmidb 73%, n = 20) than in SAT (mean CV of: ndb 23%, nmidb 55%). A second calculation was performed excluding pixels at the boundaries of the mask and pixels with an estimation of T2* under 10 ms and permitted to reduce the intra-subject variability (mean CV of ndb 22%, nmidb 52% n = 20 for VAT and ndb 16%, nmidb 33% n = 20 for SAT). The mean percentage of pixels at the boundaries of the mask was 27% for SAT and 39% for VAT. 17% pixels of SAT and 24%

pixels of VAT had an estimated T2* under 10 ms. The mean CV of MRS measurement was lower in SAT (ndb 3%, nmidb 5%, n = 20) than in VAT (ndb 11%, nmidb 21%, n = 16).

FA Composition: Comparison MRS And CSE-MRI (Whole Volume)

MRS and whole-volume CSE-MRI FA composition estimations were correlated (SAT: $r = 0.82$, $p < 0.001$ for ndb and $r = 0.84$, $p < 0.001$ for nmidb, n = 19) with a low bias (0.06 IC 95 % [-0.32 0.43] for ndb and 0.02 IC 95% [-0.15 0.20] for nmidb). It was however difficult to compare these two methods without considering the high spatial variability (intra-subject variability) of CSE-MRI measurements. As illustrated in Figure 5, the MRS value was included in the range defined by the mean ± one standard deviation of CSE-MRI measurements for each subject.

FA Composition: SAT And VAT

Regarding CSE-MRI results from the whole segmented volume (L2 to L4) versus the localized-MRS results, the comparison of FA composition of SAT and VAT appeared to be substantially equivalent in average for ndb and nmidb measurements (CSE-MRI SAT vs VAT: ndb = 2.43 ± 0.16 vs 2.20 ± 0.15 $p < 0.001$, nmidb = 0.56 ± 0.07 vs 0.46 ± 0.07 $p < 0.001$; MRS: ndb = 2.48 ± 0.29 vs 1.90 ± 0.63 $p = 0.001$, nmidb = 0.58 ± 0.14 vs 0.37 ± 0.22 $p = 0.001$) and for $PUFA_{indx}/MUFA_{indx}/SFA_{indx}$ measurements (Figure 6). In both cases, paired t-tests showed significant difference between SAT and VAT FA composition ($p < 0.001$ for CSE-MRI measurements and $p < 0.01$ for MRS measurements). The inter-subject variability was higher in localized-MRS measurements than in the CSE-MRI measurements.

FA Composition: Change Between The Two Examinations

The same trend for the variations of all the FA composition parameters was observed based on both CSE-MRI and MRS measurements for VAT (figure 7). The low inter-subject variability of CSE-MRI measurement permitted to detect significant variation of adipose

tissue composition whereas MRS measurement did not (VAT MUFA + 1.22 percentage points ($p < 0.001$) for CSE-MRI, + 0.96 percentage points ($p = 0.318$) for MRS).

FA Composition: GC-MS Analysis

Thirteen samples of SAT were analyzed using gas chromatography (7 before and 6 after the overfeeding intervention). Results were expressed as molar percentage and are presented in Table 3. Measurements by GC-MS were considered as reference.

Good correlations were found between GC-MS and CSE-MRI measurements (for ndb: r=0.84, y=0.76x+0.40, p=0.001; for nmidb: r=0.66, y=0.88x–0.09, p=0.020). However CSE-MRI measurements overestimated ndb (Bland-Altman bias=0.17 percentage points, IC 95% [0.01;0.34],) and nmidb (Bland-Altman bias=0.16 percentage points, IC 95% [0.04;0.27],). Better correlations were found between GC-MS and MRS measurements (for ndb: r=0.83, y=0.31x+1.47, p<0.001; for nmidb: r=0.74, y=0.36x+0.19, p=0.006) however the bias was larger. MRS measurements overestimated ndb (bias=0.24 percentage points, IC 95% [-0.22;0.70], Bland-Altman) and nmidb (bias=0.19 percentage points, IC 95% [- 0.04;0.42], Bland-Altman).

DISCUSSION

Consistent with the literature (24), we found that CSE-MRI-based fat mass measurements of android region is strongly correlated with DEXA measurements. However, a small bias was observed with slight lower value of TAT volume with CSE-MRI measurements. The DEXA measurement is a 2D measurement and does not permit to distinguish VAT, SAT and other ectopic fat like bone marrow and intramuscular adipose tissue. The automated segmentation processing based on CSE-MRI images enabled to separate VAT from SAT. Thus, muscles and bone marrow were excluded from VAT mask by a threshold empirically defined at 55% using the PDFF mapping. This exclusion could explain the difference in CSE-MRI and

DEXA measurements as when we considered the PDFF of muscles, vertebrae and VAT in the calculation of fat content, the bias reduced. To go further in the segmentation of different adipose tissue depots, some studies (25, 26) differentiated the deep (DSAT) from the superficial (SSAT) subcutaneous adipose tissue in the abdominal region. This segmentation of DSAT and SSAT is very challenging because the fascia superficial separating these tissues appears subtle and discontinuous and need a fine resolution (~1.25 mm). The present in-plane resolution was due to a compromise between an acquisition time compatible with breath-holding and the size of the covering volume (320 mm in the head-foot direction in this study) to give a good SNR which is an essential parameter to estimate the FA composition (i.e. proportions of $PUFA_{indx}$, $MUFA_{indx}$ and SFA_{indx}). From a metabolic point of view, GC analysis of SSAT and DSAT in a large cohort shows homogenous FA composition in the two adipose tissue depots (7).

Liver PDFF results were consistent with the literature (13–15), with a good correlation established between MRS and CSE-MRI measurements. However, some studies (13–15) provided a better correlation. It should be noted that the range of values was larger in these papers (0 – 40 % (13–15)) than in the present paper (0 – 12 %). Especially, it is challenging to accurately estimate very low fat content in liver. Here, we demonstrated that even if the PDFF measurement methods with CSE-MRI or MRS were different, the difference between the two PDFF measurements (before and after the overfeeding) was equivalent with the two methods. In this study, no T2 correction was applied on the calculation of fat content in the liver for MRS measurement. In addition, MRI method include by a priori knowledge eight fat spectral component in the quantification model, that was not the case for MRS since fat quantities were too low in this study. These could explain why the MRS measurement gave underestimated values compared to CSE-MRI measurement. On the other hand, the CSE-MRI PDFF estimate could be affected by the low SNR.

The lipid quantification by CSE-MRI could be interesting in longitudinal clinical studies, as an indirect marker of AT metabolism. Here, the average on the whole segmented volume (between L2-L4) seemed to give results consistent with the literature. Machann et al. (27) reported similar results even if they computed different FA composition indexes: the polyunsaturated index (PUI = diacyl-methyl ratio) and the unsaturated index (UI = olefinic-methyl ratio), VAT was composed by 14.9%/48.9%/36.2% of $PUFA_{indx}$/$MUFA_{indx}$/SFA_{indx} (vs 15.3%/42.7%/43.0% in our study), SAT was composed by 16.2%/56.6%/27.2% (vs 18.6%/43.7%/37.7% in our study). Other studies reported higher values of nmidb both using MRS method (0.75 SCAT calf (28), 0.687/0.745 for VAT/DSAT (26), 0.71 for SCAT leg (11), 0.79/0.81 for VAT/DSAT (12) than 0.37/0.58 for VAT/SAT in our study) and with MRI method (0.836/0.936 for VAT/SAT (10), 0.71/0.73 for VAT/DSAT (12), 0.74 for SCAT leg (11) than 0.46/0.56 for VAT/SAT in our study) which led to an estimation of PUFA superior to 20%. However, several gas chromatography analysis have quantified a lower content of PUFA (12.3% (29), 14.4% (30), 16.5% (9), 14.1%(31)) and lower nmidb (0.45(30), 0.50 (9), 0.63 (32)) which was more consistent with our present results. It should also be noted that the $PUFA_{indx}$ calculation made from *nmidb*, was not an absolute quantification but a coherent index of polyunsaturation, leading to consistent results when the most frequently identified PUFA is di-unsaturated FA. It could be possible to quantify the proportion of PUFA more precisely by calculating the proportion of omega-3 (33–35) and correcting the present calculation but it does not permit to know exactly the number of double bonds per chain.

The validation of lipid quantification by CSE-MRI using MRS measurement is a difficult task. As expected, the lipid quantification by MRS is challenging and results depend on the B0 field heterogeneities (26), the MRS sequences (36), the acquisition parameters (long TE or short TE) (29) and the fitting approaches (37). It is therefore difficult to use it as reference. On the other hand, a gold standard like gas chromatography-mass spectrometry analysis is

460 difficult to perform on human volunteers, for ethical reasons only subcutaneous adipose tissue
461 can be analyzed. In this study, good correlations were found between MRS and CSE-MRI
462 measurement, MRS and GC-MS measurements and between CSE-MRI and GC-MS
463 measurements. However, the NMR methodologies gave biased results compare to GC-MS
464 methodology. The CSE-MRI and MRS fitting approach used strong constraint on a relation
465 between ndb and nmidb (10, 19) to improve the repeatability of measurements, however this
466 constraint provided biased results and not absolute quantification. Therefore, the good
467 correlation between GC-MS and NMR methodologies is already an important result, even if, a
468 comparative study using more sample should be necessary. The higher inter-subject
469 variability seen in localized-MRS measurements compared with the CSE-MRI measurements
470 could be explained first by the difficulty to locate in some lean volunteers, the MRS voxel
471 into AT only. This could induce some partial volume effects. Moreover, due to the large
472 difference between the elementary volume (8000 mm3 for MRS compared to 9.84 mm3 for
473 MRI), the local inhomogeneity is in favor of CSE-MRI despite a dedicated localized shim for
474 MRS. Finally, the value estimated by CSE-MRI resulted from an averaging over a large
475 number of pixels (>10000 pixels) which attenuated the effect of potential aberrant individual
476 values for each subjects, unlike for the MRS where only two measurements were made. The
477 spatial non-uniformity of nmidb was larger in VAT than in SAT. This high spatial variability
478 could be due to a sensitivity of CSE-MRI FA composition measurements to local field
479 inhomogeneity as the coefficient of variation reduced when we removed pixels located at fat-
480 air interface. This local field inhomogeneity is due to high contribution of internal field as
481 regard to fat-tissue interface where susceptibility gradient is strong. To increase spatial
482 resolution may probably minimize this effect. Alternatively, to provide more consistent
483 measurements, it is possible to suppress these voxels in the segmentation pipeline such as
484 proposed in this study. Moreover, VAT tissue could be more impacted by local field

inhomogeneity due to the presence of air in the gut. In localized area, this sensitivity to local field heterogeneities led to erroneous values of CSE-MRI measurements. For the study of localized area, localized-MRS seemed to still be the best method thanks to shim methods allowing to homogenize locally the magnetic field. Visual analysis of spectrum permits to validate results with consistent fitting approach. Moreover, in the literature, only methods of spectroscopy make the quantification of omega-3 possible (33–35). A limitation of our study concerned the design of the overfeeding. This was a short term 31-days overfeeding, and as the half-life of subcutaneous adipose tissue fatty acids is around 6 to 9 months (9), the overfeeding may have been too short to detect a change in SAT fatty composition with the diet.

To conclude, significant increase in fat distribution in VAT, SAT and liver were measured by DEXA, MRS and CSE-MRI measurements after an experimental overfeeding. FA composition changes (more precisely the MUFA proportion) of the adipose tissue were also observed by CSE-MRI measurements. The use of a single 3D CSE-MRI sequence associated with a dedicated post processing method is a suitable protocol to follow several parameters linked to adipose tissue changes. This NMR protocol could be used in future work to evaluate non-invasively the impact of nutrition on adipose tissues and liver.

Acknowledgments:

This study was conducted as part of the LABEX PRIMES (ANR-11-LABX-0063) of the "Université de Lyon", within the "Investissements d'Avenir" program (ANR-11-IDEX-0007) operated by the French National Research Agency (ANR). This study was also supported by the IHU OpéRa (ANR-10-IBHU-0004), within the "Investissements d'Avenir"program operated by the French National Research Agency (ANR). We thank Corinne Louche-Pelissier and Adeline Cestre (CRNH-RA) for technical assistance in the fatty acid analyse using GC-MS.

References

1. Heymsfield SB, Wadden TA: Mechanisms, Pathophysiology, and Management of Obesity. *N Engl J Med* 2017; 376:254–266.

2. Lee JJ, Pedley A, Hoffmann U, Massaro JM, Levy D, Long MT: Visceral and Intrahepatic Fat Are Associated with Cardiometabolic Risk Factors Above Other Ectopic Fat Depots: The Framingham Heart Study. *Am J Med* 2018; 131:684-692.e12.

3. Alligier M, Gabert L, Meugnier E, et al.: Visceral Fat Accumulation During Lipid Overfeeding Is Related to Subcutaneous Adipose Tissue Characteristics in Healthy Men. *J Clin Endocrinol Metab* 2013; 98:802–810.

4. Chowdhury B, Sjöström L, Alpsten M, Kostanty J, Kvist H, Löfgren R: A multicompartment body composition technique based on computerized tomography. *Int J Obes Relat Metab Disord J Int Assoc Study Obes* 1994; 18:219–234.

5. Hu HH, Kan HE: Quantitative proton MR techniques for measuring fat. *NMR Biomed* 2013; 26:1609–1629.

6. Reeder SB, Hu HH, Sirlin CB: Proton density fat-fraction: A standardized mr-based biomarker of tissue fat concentration. *J Magn Reson Imaging* 2012; 36:1011–1014.

7. Petrus P, Edholm D, Rosqvist F, et al.: Depot-specific differences in fatty acid composition and distinct associations with lipogenic gene expression in abdominal adipose tissue of obese women. *Int J Obes* 2017; 41:1295–1298.

8. Jové M, Moreno-Navarrete JM, Pamplona R, Ricart W, Portero-Otín M, Fernández-Real JM: Human omental and subcutaneous adipose tissue exhibit specific lipidomic signatures. *FASEB J* 2013; 28:1071–1081.

9. Hodson L, Skeaff CM, Fielding BA: Fatty acid composition of adipose tissue and blood in humans and its use as a biomarker of dietary intake. *Prog Lipid Res* 2008; 47:348–380.

10. Leporq B, Lambert SA, Ronot M, Vilgrain V, Van Beers BE: Quantification of the triglyceride fatty acid composition with 3.0 T MRI. *NMR Biomed* 2014; 27:1211–1221.

11. Peterson P, Månsson S: Simultaneous quantification of fat content and fatty acid composition using MR imaging. *Magn Reson Med* 2013; 69:688–697.

544 12. Bydder M, Girard O, Hamilton G: Mapping the double bonds in
545 triglycerides. *Magn Reson Imaging* 2011; 29:1041–1046.

546 13. Achmad E, Yokoo T, Hamilton G, et al.: Feasibility of and agreement
547 between MR imaging and spectroscopic estimation of hepatic proton density fat
548 fraction in children with known or suspected nonalcoholic fatty liver disease.
549 *Abdom Imaging* 2015; 40:3084–3090.

550 14. Zand KA, Shah A, Heba E, et al.: Accuracy of multiecho magnitude-based
551 MRI (M-MRI) for estimation of hepatic proton density fat fraction (PDFF) in
552 children. *J Magn Reson Imaging* 2015; 42:1223–1232.

553 15. Tyagi A, Yeganeh O, Levin Y, et al.: Intra- and inter-examination
554 repeatability of magnetic resonance spectroscopy, magnitude-based MRI, and
555 complex-based MRI for estimation of hepatic proton density fat fraction in
556 overweight and obese children and adults. *Abdom Imaging* 2015; 40:3070–3077.

557 16. Stults-Kolehmainen MA, Stanforth PR, Bartholomew JB, Lu T, Abolt CJ,
558 Sinha R: DXA estimates of fat in abdominal, trunk and hip regions varies by
559 ethnicity in men. *Nutr Diabetes* 2013; 3:e64.

560 17. Folch J, Lees M, Sloane Stanley GH: A simple method for the isolation and
561 purification of total lipides from animal tissues. *J Biol Chem* 1957; 226:497–
562 509.

563 18. Gabert L, Vors C, Louche-Pélissier C, et al.: 13C tracer recovery in human
564 stools after digestion of a fat-rich meal labelled with [1,1,1-13C3]tripalmitin and
565 [1,1,1-13C3]triolein. *Rapid Commun Mass Spectrom* ; 25:2697–2703.

566 19. Nemeth A, Segrestin B, Leporq B, et al.: Comparison of MRI-derived vs.
567 traditional estimations of fatty acid composition from MR spectroscopy signals.
568 *NMR Biomed* 2018; 31:e3991.

569 20. Ratiney H, Bucur A, Sdika M, Beuf O, Pilleul F, Cavassila S: Effective voigt
570 model estimation using multiple random starting values and parameter bounds
571 settings for in vivo hepatic 1H magnetic resonance spectroscopic data. In *2008*
572 *5th IEEE Int Symp Biomed Imaging Nano Macro*; 2008:1529–1532.

573 21. Leporq B, Ratiney H, Pilleul F, Beuf O: Liver fat volume fraction
574 quantification with fat and water T1 and T2* estimation and accounting for
575 NMR multiple components in patients with chronic liver disease at 1.5 and 3.0
576 T. *Eur Radiol* 2013; 23:2175–2186.

577 22. Lankton S, Tannenbaum A: Localizing Region-Based Active Contours.
578 *IEEE Trans Image Process* 2008; 17:2029–2039.

579 23. Snyder W, Cook M, Nasset E, Karhausen L, Parry Howells G, Tipton I:
580 Report of the Task Group on Reference Man. International Commission on
581 radiological protection, no. 23. Pergamon Press: Oxford; 1975.

582 24. Silver HJ, Niswender KD, Kullberg J, et al.: Comparison of Gross Body Fat-
583 Water Magnetic Resonance Imaging at 3 Tesla to Dual Energy X-Ray
584 Absorptiometry in Obese Women. *Obes Silver Spring Md* 2013; 21:765.

585 25. Sadananthan SA, Prakash B, Leow MK-S, et al.: Automated segmentation of
586 visceral and subcutaneous (deep and superficial) adipose tissues in normal and
587 overweight men. *J Magn Reson Imaging* 2015; 41:924–934.

588 26. Hamilton G, Schlein AN, Middleton MS, et al.: In vivo triglyceride
589 composition of abdominal adipose tissue measured by 1H MRS at 3T. *J Magn*
590 *Reson Imaging* 2017; 45:1455–1463.

591 27. Machann J, Stefan N, Wagner R, et al.: Intra- and interindividual variability
592 of fatty acid unsaturation in six different human adipose tissue compartments
593 assessed by 1H-MRS in vivo at 3 T. *NMR Biomed* 2017; 30:e3744.

594 28. Ren J, Dimitrov I, Sherry AD, Malloy CR: Composition of adipose tissue
595 and marrow fat in humans by 1H NMR at 7 Tesla. *J Lipid Res* 2008; 49:2055–
596 2062.

597 29. Lundbom J, Hakkarainen A, Fielding B, et al.: Characterizing human
598 adipose tissue lipids by long echo time 1H-MRS in vivo at 1.5 Tesla: validation
599 by gas chromatography. *NMR Biomed* 2010; 23:466–472.

600 30. Field CJ, Angel A, Clandinin MT: Relationship of diet to the fatty acid
601 composition of human adipose tissue structural and stored lipids. *Am J Clin Nutr*
602 1985; 42:1206–1220.

603 31. Rosqvist F, Iggman D, Kullberg J, et al.: Overfeeding Polyunsaturated and
604 Saturated Fat Causes Distinct Effects on Liver and Visceral Fat Accumulation in
605 Humans. *Diabetes* 2014; 63:2356–2368.

606 32. Garaulet M, Hernandez-Morante JJ, Lujan J, Tebar FJ, Zamora S:
607 Relationship between fat cell size and number and fatty acid composition in
608 adipose tissue from different fat depots in overweight/obese humans. *Int J Obes*
609 2006; 30:899–905.

610 33. Lundbom J, Heikkinen S, Fielding B, Hakkarainen A, Taskinen M-R,
611 Lundbom N: PRESS echo time behavior of triglyceride resonances at 1.5T:
612 Detecting ω-3 fatty acids in adipose tissue in vivo. *J Magn Reson* 2009; 201:39–
613 47.

614 34. Fallone CJ, McKay RT, Yahya A: Long TE STEAM and PRESS for
615 estimating fat olefinic/methyl ratios and relative ω-3 fat content at 3T. *J Magn*
616 *Reson Imaging* 2018; 48:169–177.

617 35. Škoch A, Tošner Z, Hájek M: The in vivo J-difference editing MEGA-
618 PRESS technique for the detection of n-3 fatty acids. *NMR Biomed* 2014;
619 27:1293–1299.

620 36. Hamilton G, Middleton MS, Bydder M, et al.: Effect of PRESS and STEAM
621 sequences on magnetic resonance spectroscopic liver fat quantification. *J Magn*
622 *Reson Imaging* 2009; 30:145–152.

623 37. Mosconi E, Sima DM, Osorio Garcia MI, et al.: Different quantification
624 algorithms may lead to different results: a comparison using proton MRS lipid
625 signals. *NMR Biomed* 2014; 27:431–443.

626

627

Tables

Table 1. Parameters conditioning the fat spectrum model used				
Component k	Type	Δf_k (Hz)	Chemical shift (ppm)	n_k(ndb,nmidb,CL)
1	Olefinic + Glycerol	-74.9	5.29 5.19	2 x ndb +1
water	-	0	4.70	$n_{water} = 2$
2	Glycerol	63.5	4.20	4
3	Dyacil	247.7	2.75	2 x nmidb
4	α-carboxyl	312.4	2.24	6
5	α-olefinic	340.4	2.02	4 x (ndb-nmidb)
6	β-carboxyl	393.7	1.60	6
7	Methylene	431.8	1.30	6x(CL-4)-8 x ndb + 2 x nmidb
8	Methyl	482.6	0.90	9

Table 1: Parameters conditioning the fat spectrum model used. Δf_k, frequency shift between water and each fat resonance.

	Baseline	After the overfeeding intervention	Differences
Age	33±2		
Body weight(kg)	79.6±1.6	82.4±1.6	2.6±0.3*** (n = 21)
Body Mass index (kg/m^2)	25.2±0.3	26.0±0.3	0.8±0.1*** (n = 21)
DEXA			
fat mass of whole body (kg)	19.6±1.2	21.2±1.1	1.6±1.1*** (n = 21)
fat mass of android region (kg)	1.85±0.13	2.07±0.57	0.19±0.04** (n = 20, p=0.001)
CSE-MRI			
SAT volume(cm^3)	1104±74	1191±79	91±22*** (n=20)
VAT volume (cm^3)	922±104	1070±116	129±31*** (n=20)
TAT volume (cm^3)	2027±745	2261±765	219±41*** (n=20)
VAT/SAT	0,83±0,08	0,91±0,09	0,06±0,03* (n=20, p=0.020)
liver PDFF	2.70±0.54	4.05±0.87	1.35±0.39** (n=20, p=0.003)
localized liver PDFF	1.73± 0.34	3.38 ± 0.77	1.66 ± 0.53** (n=19, p=0.006)

FA composition of SAT	ndb = 2.43 ± 0.04	2.43 ± 0.03	0.00 ± 0.01 (n=19, p=0.812)
	nmidb = 0.56 ± 0.02	0.55 ± 0.01	0.00 ± 0.01 (n=19, p=0.612)
FA composition of VAT	ndb = 2.20 ± 0.03	2.19 ± 0.03	-0.01 ± 0.02 (n=19, p=0.512)
	nmidb = 0.46 ± 0.02	0.44 ± 0.01	-0.03 ± 0.01* (n=19, p=0.013)
MRS			
liver PDFF	1.20± 0.23	3.02± 0.31	1.74±0.48** (n=20, p=0.002)
FA composition of SAT	ndb = 2.48 ± 0.06	2.45 ± 0.07	-0.05± 0.05 (n=20, p=0.381)
	nmidb = 0.58 ± 0.03	0.57 ± 0.03	-0.02 ± 0.03 (n=20, p=0.417)
FA composition of VAT	ndb = 1.90 ± 0.16	2.04 ± 0.11	0.19 ± 0.17 (n=15, p=0.290)
	nmidb = 0.37 ± 0.06	0.41 ± 0.04	0.06 ± 0.06 (n=15, p=0.395)

Table 2: Measurements of the cohort before and after overfeeding. Data are expressed as mean SEM. * indicate significant difference due to overfeeding paired t-test ***p<0.001. SAT: abdominal subcutaneous adipose tissue from L2 to L4; VAT: visceral adipose tissue from L2 to L4; TAT: total abdominal adipose tissue (SAT+VAT); PDFF: proton density fat fraction; FA: fatty acid; ndb, number of double bonds; nmidb, number of methylene-interrupted double bonds.

	Fatty acid	Mean	SD
SFA (%)	C12	0.80	0.17
	C14	4.99	0.48
	C15	0.47	0.03
	C16	27.40	1.31
	C18	4.32	0.63
	C20	0.12	0.02
MUFA (%)	C14:1	0.49	0.12
	C16:1	4.46	1.14
	C18:1n9t	0.47	0.08
	C18:1n9c	42.15	1.3
	C18:1n7	1.75	0.09
	C20:1	0.45	0.03
PUFA (%)	C18:2n6c	11.09	2.32
	C20:2	0.15	0.01
	C18:3n3	0.68	0.18
	C20:4n6	0.20	0.05
PUFA (%)		12.12	2.44
MUFA (%)		49.78	2.27
SFA (%)		38.10	1.98
ndb_{GC}		2.25	0.12
$nmidb_{GC}$		0.40	0.08
CL_{GC}		17.10	0.06
$PUFA_{indx}$ (%)		13.21	2.57
$MUFA_{indx}$ (%)		48.69	2.37
SFA_{indx} (%)		38.10	1.98

Table 2: Molar percentage of the different fatty acid of human subcutaneous adipose tissue determined by gas chromatography (n = 13). $PUFA_{indx}$, $MUFA_{indx}$ and SFA_{indx} were computed using ndb_{GC} and $nmidb_{GC}$.

Figure Legends

Figure 1: A STEAM sequence was acquired in liver, subcutaneous adipose tissue (SAT) and visceral adipose tissue (VAT) using the following parameters: TR = 3000 ms, TE= 14 ms, TM= 10 ms, VOI of 20×20×20 mm3, no water suppression, 2048 Hz bandwidth, 1024 data points, 4 signal averages for VAT and SAT and 32 signal averages for the liver. For SAT and VAT, further acquisitions were made with TE = [24, 34, 44, 54, 64] ms.

Figure 2: The total abdominal adipose tissue (TAT) volume delimited by the lumbar vertebrae L2 and L4 was calculated using CSE-MRI. This volume was converted into mass using the assumed density of 0.92 g/cm3 and compared to the DEXA measurement on android region. The dotted line in the left part of this graph represents the identity line.

Figure 3: Dots represent the value of the proton density fat fraction (PDFF) in the liver for each subject and are represented in a boxplot beside dots. Figures a) and b) show CSE-MRI measurements. Figures c) and d) show MRS measurements. In figures a) and c) data before overfeeding (MRI1 and MRS1) are in pink color and data after the overfeeding (MRI2 and MRS2) in blue. In figures b) and d) the difference between the two examinations was illustrated. Paired t-test was performed between MRI1 and MRI2 for the PDFF in the liver. Significant difference between the two examinations was shown by Paired t-test (** p-value < 0.01) and Wilcoxon rank test ($p<0.001$), n = 20, . The PDFF increased significantly (+ 1.35, p = 0.002 for CSE-MRI measurements; + 1.74, p = 0.002 for MRS measurements).

Figure 4: The left part of this graph shows a good correlation between ΔMRI (localized MRI2-MRI1 measurement) and ΔMRS (MRS2-MRS1 measurement). The Pearson's coefficient was $r = 0.88$, $p < 0.001$. The Bland-Altman in the right part of the graph shows a little bias of 0.05.

Figure 5: For each subject (n = 21, baseline examination, abdominal subcutaneous adipose tissue), the mean value of ndb (a) and nmidb (b) is in red color for CSE-MRI measurement and in black for MRS measurement. The error bars represent the standard deviation in the whole volume studied for CSE-MRI measurements and the mean deviation between the MRS test-retest measurements. The CSE-MRI measurements of subject '1' were missing. The MRS measurements of subject '20' were missing.

Figure 6: Bars represent the mean value of PUFAindx (resp. MUFAindx and SFAindx) and error bars represent the standard deviation (inter-subject variability) for the tissue VAT (visceral adipose tissue) and SAT (abdominal subcutaneous adipose tissue) measured a) by MRS and b) by CSE-MRI method. Paired t-tests were performed between values from SAT against values from VAT for PUFAindx, MUFAindx and SFAindx measurements. *** $p < 0.001$, ** $p < 0.01$.

Figure 7: Dots represent the difference between the baseline measurement and after the overfeeding. The inter-subject of MRS measurement was higher than CSE-MRI measurement. Paired t-tests were performed between the two examinations (SAT: PUFAindx/MUFAindx/SFAindx - 0.12 ($p = 0.356$)/0.34 ($p = 0.001$)/-0.23 ($p = 0.356$) n = 19 for CSE-MRI and -0.94 ($p = 0.416$)/-0.20 ($p = 0.314$)/ 1.15 ($p = 0.354$) n = 18 for MRS; VAT: -0.84 ($p = 0.012$)/1.22 ($p < 0.001$)/-0.38 ($p = 0.349$) n = 19 for CSE-MRI and -0.38 ($p = 0.604$)/0.96 ($p = 0.318$)/ -0.58 ($p = 0.443$) n = 13 for MRS).

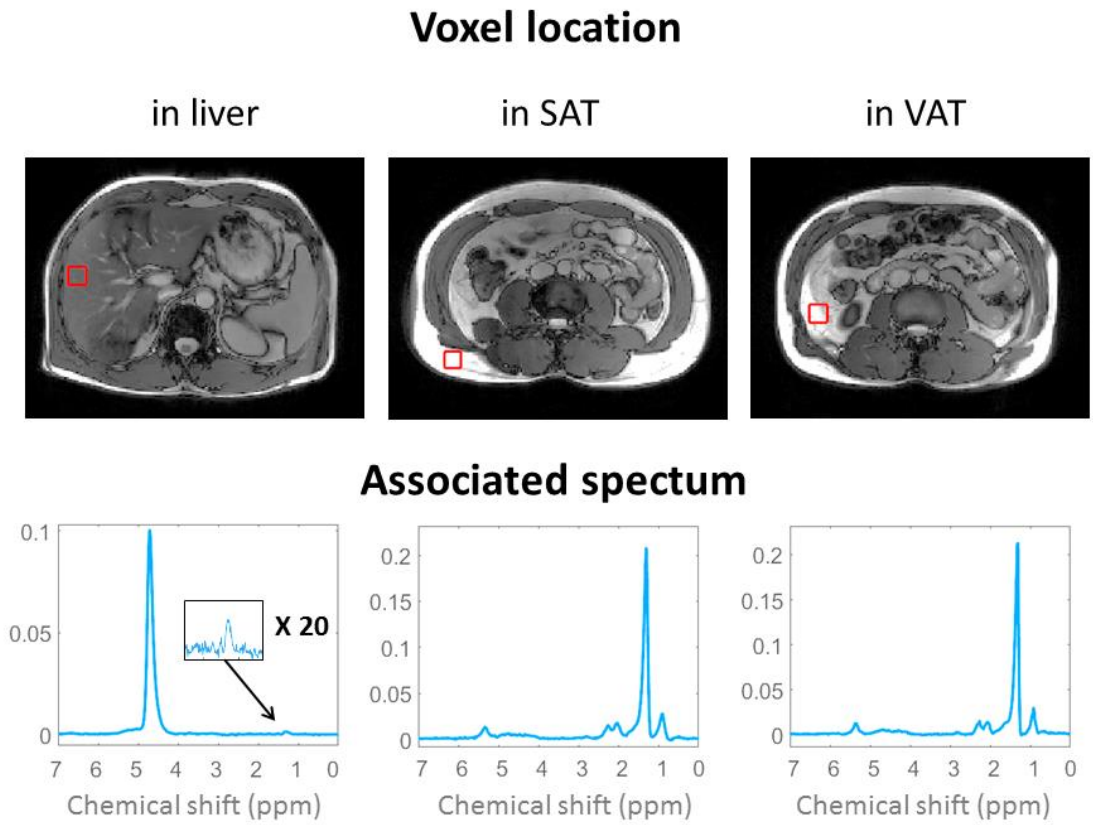

684

685 **Figure 1**

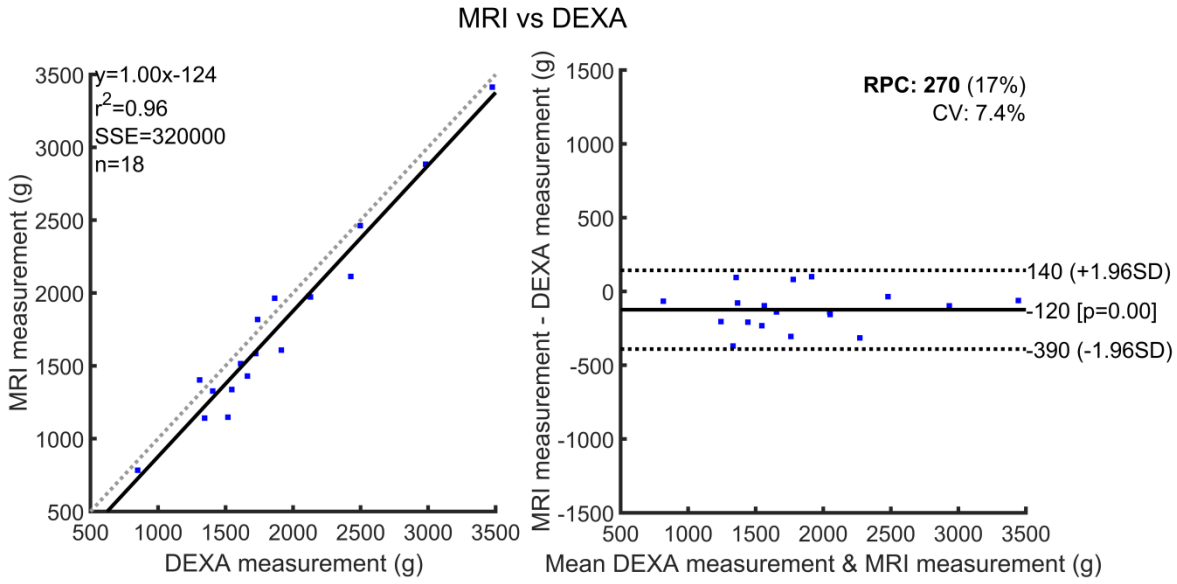

686

687 **Figure 2**

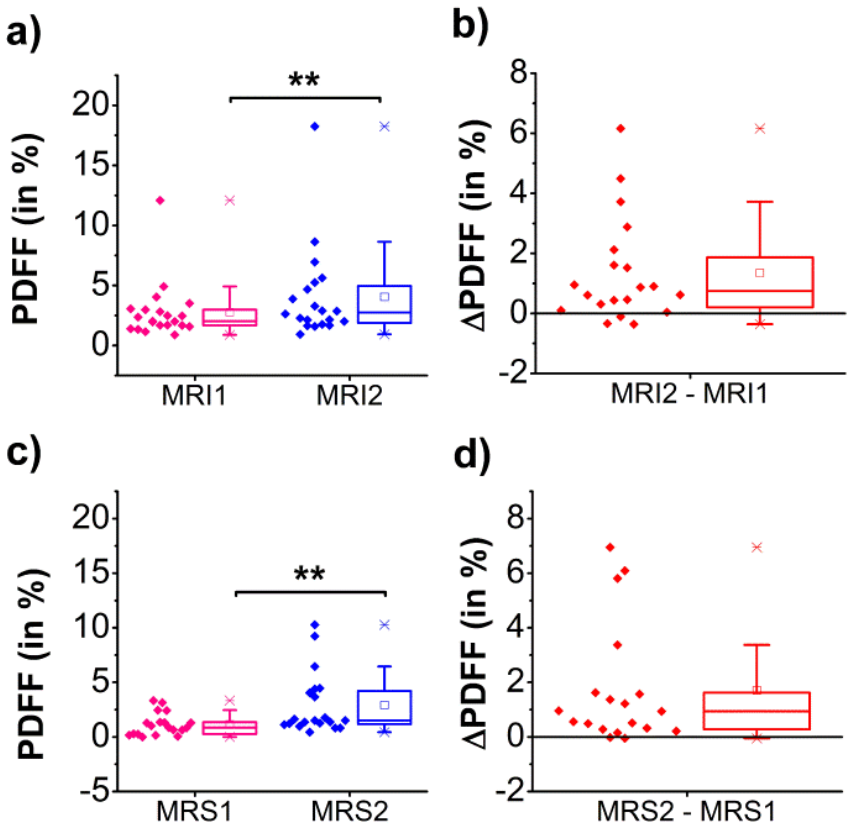

688

689 **Figure 3**

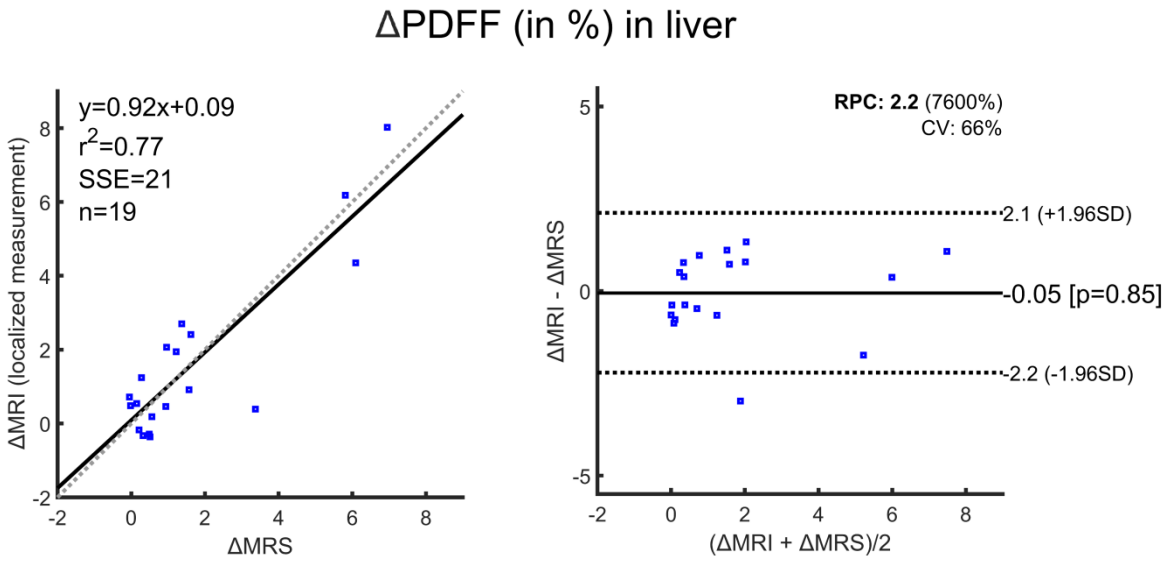

690

691 **Figure 4**

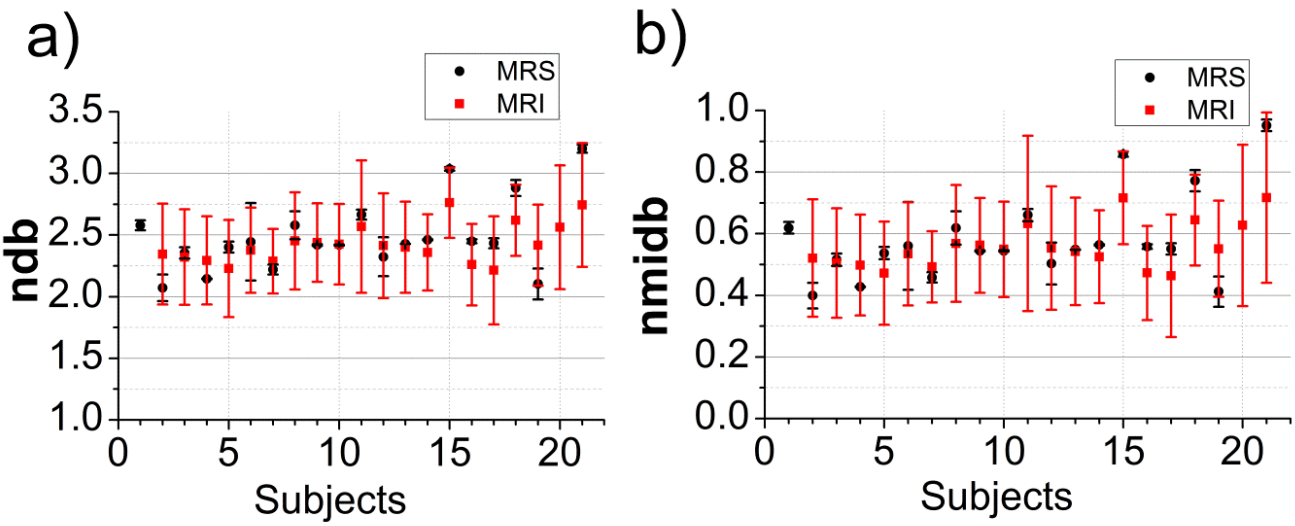

692

693 **Figure 5**

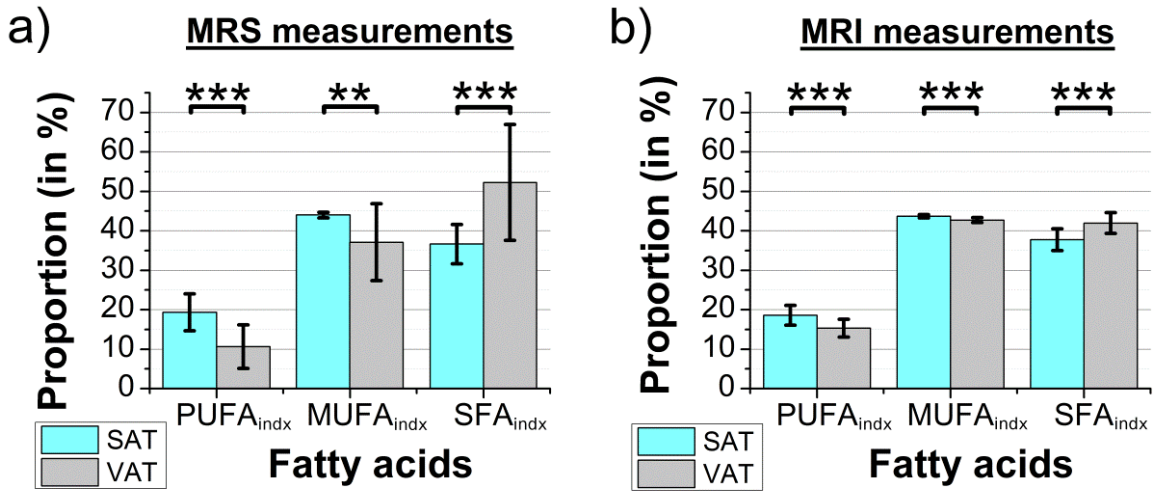

694

695 **Figure 6**

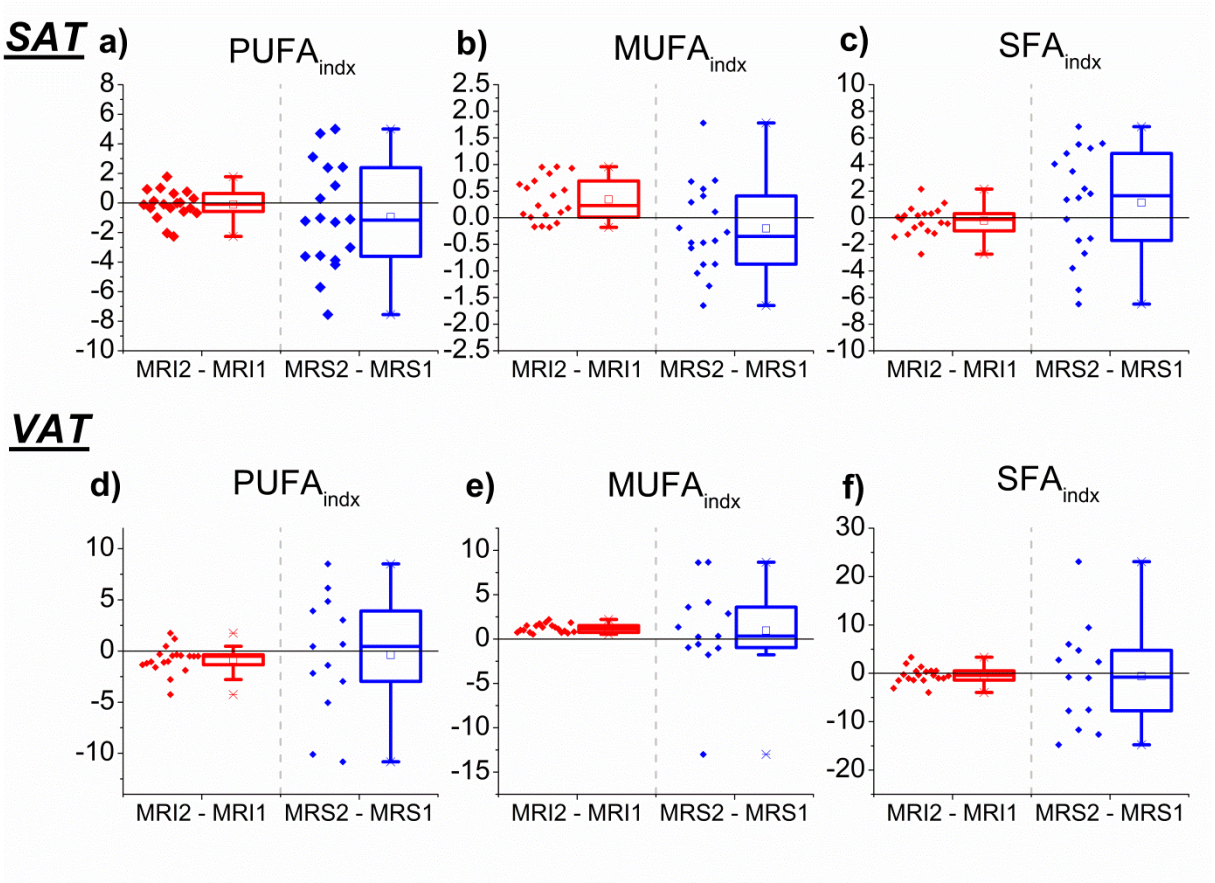

696

697 **Figure 7**

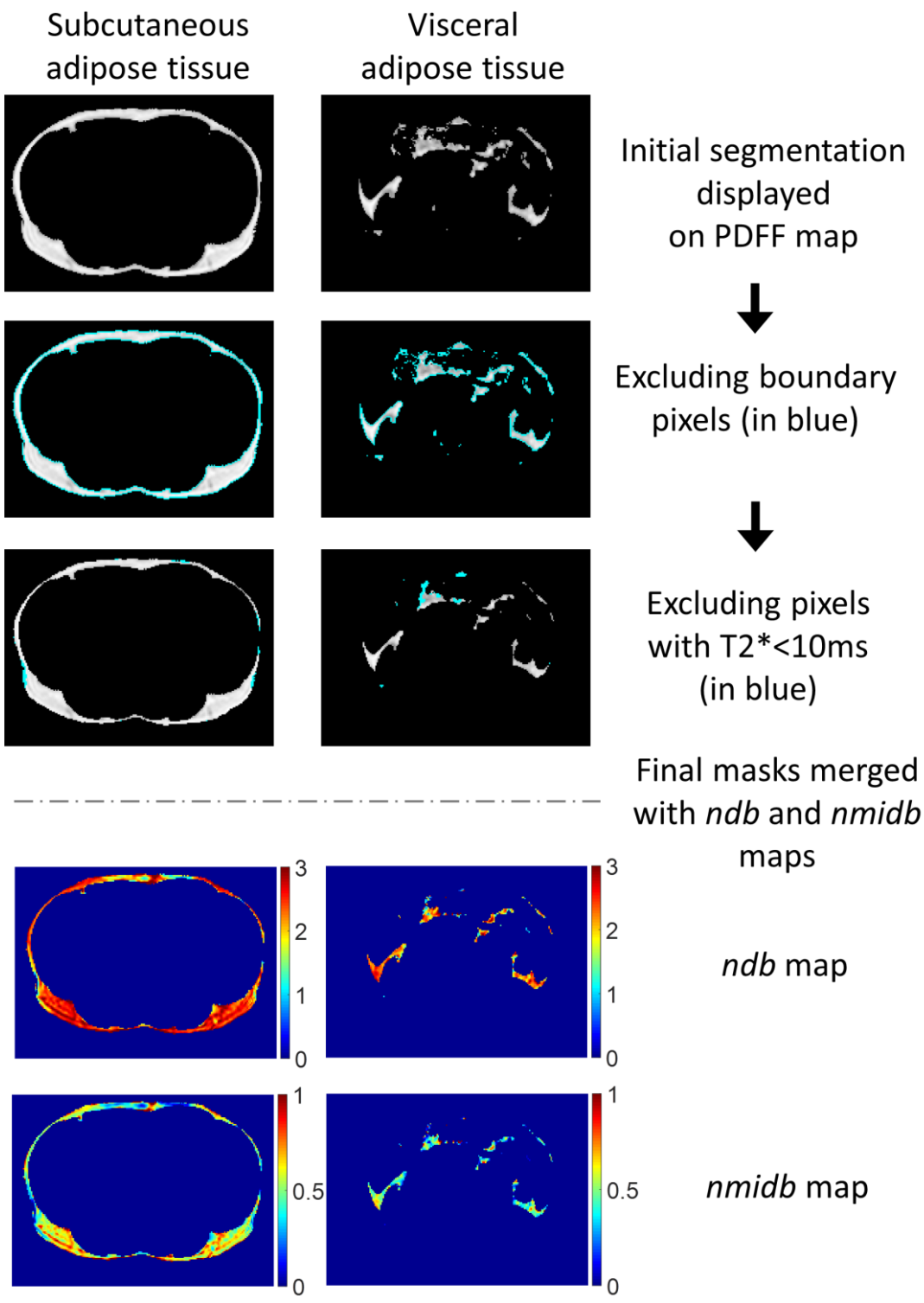

Supplementary figure 1: Procedure of pixel exclusion after the initial segmentation to compute the mean ndb (number of double bonds) and nmidb (number of methylene-interrupted double bonds). Pictures in grey scale are displaying the subcutaneous and visceral adipose tissue masks merged with the PDFF maps. Pictures in color scale are displaying the subcutaneous and visceral adipose tissue masks merged with the ndb and nmidb maps.

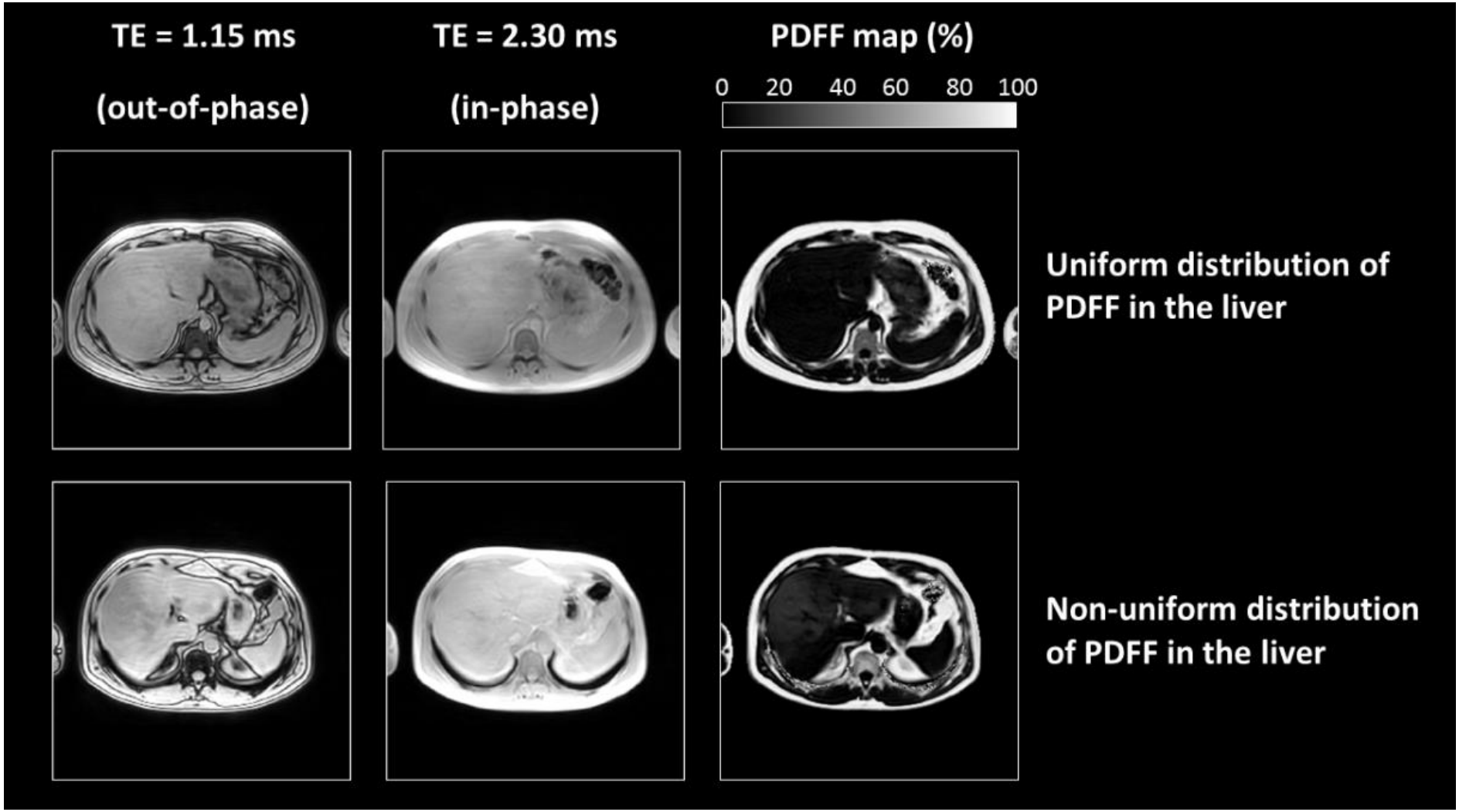

Supplementary figure 2: Two examples of exams with different PDFF distribution in the liver. 3D MRI acquisition parameters were the following : 8 echoes (n x 1.15 ms TE with n=1, …,8), 5° flip angle, 10.3 ms TR, 384 x 420 x 320 mm3 FOV, 256 x 256 x 80 matrix size, 20.8 s scan time. This acquisition was made in breath-holding. The first (out of phase) and second (in-phase) echoes as well as the PDFF map are displayed.